Chapter 6

Wind Tunnel Tests on Horn-Shaped Membrane Roof Under the Turbulent Boundary Layer

Yuki Nagai, Akira Okada, Naoya Miyasato,
Masao Saitoh and Ryota Matsumoto

Additional information is available at the end of the chapter

http://dx.doi.org/10.5772/54180

1. Introduction

In this paper, the authors describe about a wind tunnel test for a membrane roof on a civil engineering. Especially, the authors focused on the horn-shaped membrane roof (shown in fig.1). Wind loading is the most dominant load for light-weight structures such as membrane roofs. A wind-force coefficient of typical building type such as box-type is defined in the guideline and the cord, but a wind-force coefficient of complicated shapes such as the horn-shaped membrane roof has not been sufficiently reported yet.

In general, there are two types of wind-tunnel test on the membrane roof, namely a test using a rigid model and a test using an elastic model. The test of the rigid model is used to measure the wind pressure around the building. On the other hand, the test of the elastic model can measure the deflection of the membrane surface directly and grasp the behavior of the membrane. This paper describes about the test using the rigid model for the horn-shaped membrane roof structure to measure a wind-force coefficient and fluctuating wind pressure coefficient around membrane under the turbulent boundary layer flow.

1.1. Past research about the wind tunnel on the horn-shaped membrane structures

Wind pressure coefficients of typical building type such as box-type are defined in guidelines and standards in each country, but wind pressure coefficients of complicated shapes such as the horn-shaped membrane roof have not been sufficiently reported yet.

The basic studies, which were about the theory and the analysis method, on the horn-shaped membrane roof were reported by F. Otto, M. Saitoh et al and also were shown the wind-pressure coefficients of the horn-shaped membrane roof under regulated conditions in several

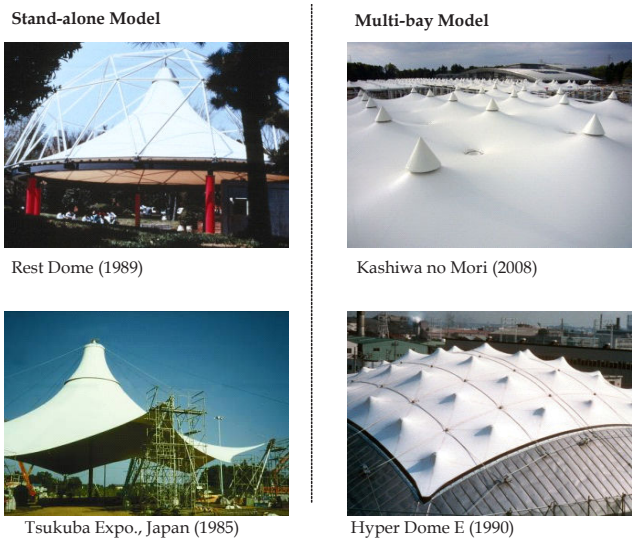

Figure 1. Horn-shaped membrane roof

reports and books (Otto, 1969; Saitoh & Kuroki, 1989; Nerdinger, 2005). In the recent years, studies on the numerical simulation against the horn-shaped membrane roof were reported by J. Ma, C. Wang et al (Ma et al., 2007; Wang et al., 2007). Furthermore, dissertation by U. Kaiser indicated wind effects on weak pre-stressed membrane structure which is 30m horn shaped membrane by aero-elastic models (Kaiser, 2004).

In this way, there are many other references on this field. However, the basic date for the wind-force coefficient of the horn-shaped membrane roof has not been sufficiently reported yet. Based on this background, the authors have carried on the wind tunnel test, and report these results.

1.2. The composition of this paper

In this chapter, the authors describe about a composition of this paper and explain three types of wind tunnel test (see fig. 2).

Chapter 2 shows a form of the horn-shaped membrane roof and example of a basic technique to form finding method of the membrane structure before the wind tunnel tests. Chapter 3 shows definitions of symbols and calculation formulas on this paper. Chapter 4 shows outline of wind tunnel device and method of measuring. Chapter 5 shows a flow condition of the test which is the turbulent boundary layer flow, and test conditions. Chapter 6 and 7 show the wind tunnel tests and the results; the test of stand-alone type model in chapter 6 and the test of multi-bay models on chapter 7. These tests indicate mean wind pressures coefficient, fluctuating wind pressure coefficient and peak wind pressure coefficient around the horn-shaped membrane structures under the turbulent boundary layer flow.

http://dx.doi.org/10.5772/54180

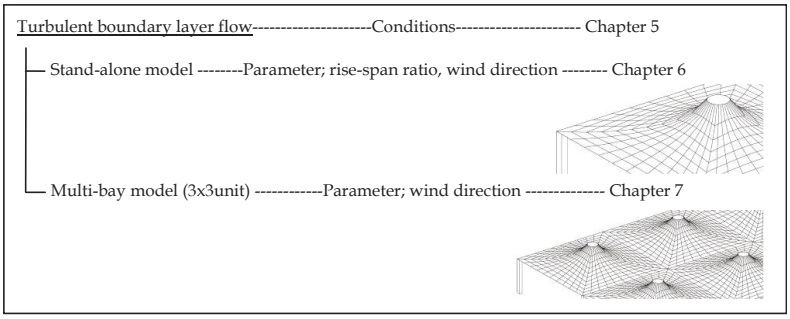

Figure 2. The composition of this paper

2. Form of the horn-shaped membrane roof

The horn-shaped membrane roofs have several kind of planar shape, namely a circle, a square and a hexagon. This paper describes about the square based horn-shaped membrane roof. In general, the membrane structure needs to find appropriate forms to resist external force. 'European Design Guide for Tensile Surface' by TensiNet presents some methods of form-finding for the membrane structures (Forster & Mollaert, 2004). This paper used nonlinear finite element method to find the appropriate form on the square based horn-shaped membrane.

In this paper, the membrane material was defined as low stiffness material (see figure 3). On the other hand, a strut was defined as high stiffness material. A strut was transferred point B from point A in order to get the appropriate form using FEM analysis. A rise-span ratio h/L was defined as the ratio of a span L to a height of the horn-shaped roof H, and an appropriate form of h/L=0.2 was obtained by finite element method with geometrical nonlinear in this paper. Additionally, the top of strut was L/10 and there wasn't a hole on the middle of the horn-shaped roof. The final shape get three-dimensional curved surface.

3. Definitions of symbols and calculation formula on this paper

The wind pressure coefficient was calculated based on *The Building Standard Law of Japan* (The building Center of Japan, 2004), *Recommendations for Load on Buildings 2004* (Architectural Institute of Japan, 2004) and *ASCE Manuals* (Cermak & Isyumov, 1998). Definitions of the symbols in this paper are shown in figure 4. As for the signs of wind pressure coefficient, the positive (+) means positive pressure against the roof and the negative (-) means negative pressure against the roof.

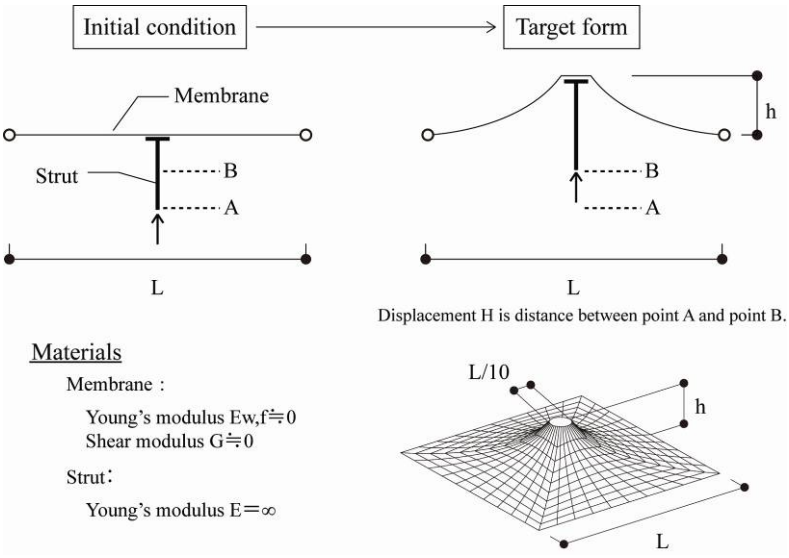

Figure 3. Form finding method on the horn-shaped membrane structure

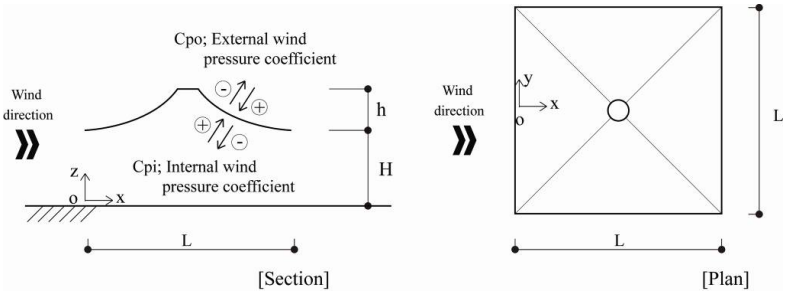

Figure 4. The definitions of symbols in this paper

The wind pressure coefficient is obtained from follows;

$$C_{pj} = C_{poj} - C_{pij} \tag{1}$$

$$C_{pij} = \frac{P_{ij} - P_S}{\bar{q}_z}, C_{poj} = \frac{P_{oj} - P_S}{\bar{q}_z} \tag{2}$$

$$\bar{q}_z = \frac{1}{2}\rho \overline{v_z}^2 \tag{3}$$

http://dx.doi.org/10.5772/54180

in which C_{pj} is the wind pressure coefficient at measurement pressure tap j, C_{poj} is the external wind pressure coefficient at measurement tap j, C_{pij} is the internal wind pressure coefficient at measurement tap j, P_{ij} is the internal pressure at measurement tap j, P_o is the external pressure at measurement tap j, P_s is the static, or the barometric, pressure at a reference location, $\bar{q}_z$ is the mean value of dynamic pressure at the reference location z, ρ is the density of the air, and $\bar{v}_z$ is the mean value of wind velocity at the reference location z. In this paper, the reference location z with the uniform flow means the position of the pitot tube. On the other hand, the reference location z with the turbulent boundary layer flow was obtained from the following equations;

$$z = h + \frac{H}{2} \tag{4}$$

in which h is the eave height of the roof, and H is the rise of the horn-shaped roof.

Particularly, the mean value of wind pressure coefficient C_{p_mean} and the peak value of wind pressure coefficient C_{p_peak} are expressed respectively as follows;

$$C_{p\_mean} = C_{po\_mean} - C_{pi\_mean} \tag{5}$$

$$\begin{cases} C_{p\_peak,\max} = C_{po\_peak,\max} - C_{pi\_peak,\min} \\ C_{p\_peak,\min} = C_{po\_peak,\min} - C_{pi\_peak,\max} \end{cases} \tag{6}$$

in which C_{po_mean} and C_{pi_mean} are the mean value of external and internal wind pressure coefficient, C_{po_peak} and C_{pi_peak} are the tip value of external and internal wind pressure coefficient.

Additionally, C_{pi_mean}, C_{po_mean}, C_{po_peak} and C_{pi_peak} are given by the following equations;

$$C_{pi\_peak} = \frac{P_{i\_mean}}{\bar{q}_z}, C_{po\_peak} = \frac{P_{o\_mean}}{\bar{q}_z} \tag{7}$$

$$C_{pi\_mean} = \frac{P_{i\_mean}}{\bar{q}_z}, C_{po\_mean} = \frac{P_{o\_mean}}{\bar{q}_z} \tag{8}$$

in which P_{i_mean} and P_{o_mean} are the mean value of internal and external wind pressure on the pressure measurement tap respectively, and P_{i_peak} and P_{o_peak} are the tip value of internal and external wind pressure on the tap. In case of the enclosed type which is constructed with side walls, P_i is neglected on these calculations.

4. Outline of wind tunnel configuration

These tests were aimed at measuring local wind pressure on the horn-shaped membrane roof using the Eiffel type wind tunnel as shown in table 1 and figure 5. The turbulent boundary layer flow was made by the roughness blocks, the spires and the trips (show in figure 6). The P_j-P_s, which P_j is the pressure at the measurement pressure tap j and P_s is the static pressure at the pitot tube, was measured directly by the laboratory pressure transducer as a differential pressure and represents the wind pressure acting at the particular pressure tap location j within the computer as sown in figure 7.

Wind tunnel	Wind tunnel facility	Eiffel type wind tunnel
	Length of wind tunnel	31000mm
	Section size	2200×1800×17300mm (width×height×length)
	Contraction ratio	1 : 3
	Velocity range	0.0~25.0
Blower	Form	GFPR's axial fan
	Wing shape	φ=2500mm
	Volume	About 100

Table 1. Outline of wind tunnel configuration

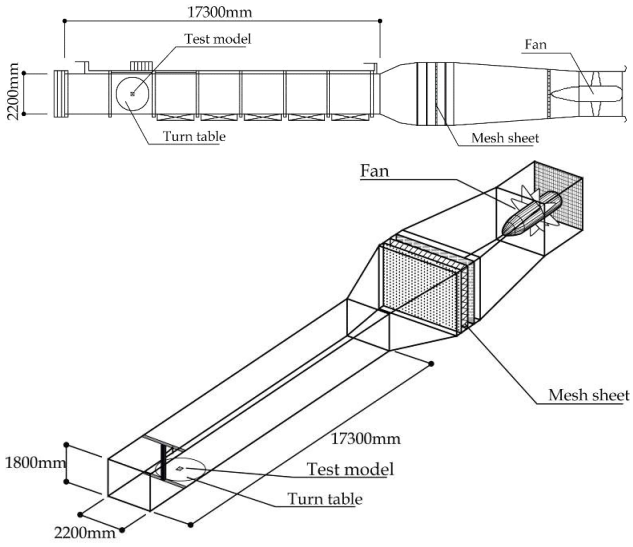

Figure 5. Sketch of Eiffel wind tunnel used

http://dx.doi.org/10.5772/54180

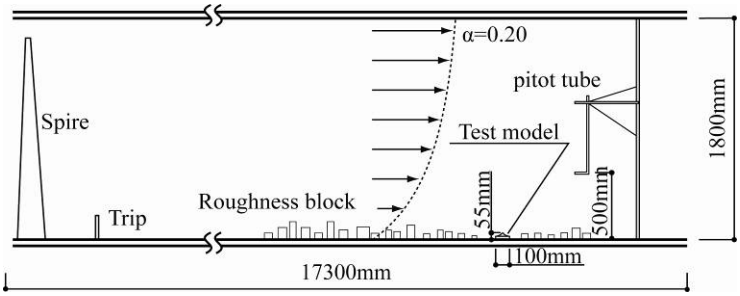

Figure 6. Cross-section diagram of wind tunnel facilities

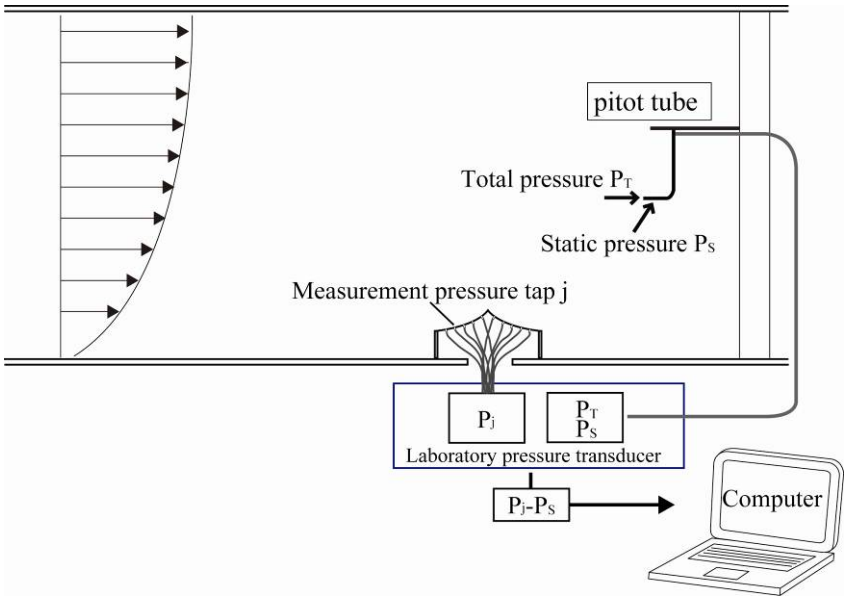

Figure 7. The wind pressure acting at the particular pressure tap location *j*

5. Outline of the turbulent boundary layer flow

In this chapter, the outline of the turbulent boundary layer flow is described. Table 2 shows conditions and parameters on the tests. It was assumed that a model scale was 1: 100 and that a velocity scale was 7/27 at the full scale wind speed 34m/s. In this case, time scale was 11/125, and additional flow conditions indicate in figure 9. Airflow conditions which were the average wind speed profile, the turbulence intensity, the power spectral density of fluctuating wind

speed and the scale of turbulence for this test, are shown in figure 9. The velocity gradient α was 0.2 and the turbulent intensity around the roof was about 0.3. This wind was simulated natural wind in the urban area, namely "terrain 3" in the Building Standard Low of Japan.

Figure 8. Photos of wind tunnel test

Flow	Boundary Turbulent Layer Flow (Urban Area; Terrain 3 in The Building Standard Law of Japan)
Wind velocity	About 7 m/s at z=35mm (around the test model)
Velocity gradient α	α=0.2
Velocity turblence intensity Ir	0.3 at z=35mm (around the test model)

Table 2. Airflow Condition on the wind tunnel

Model Type	Stand-alone model, Multi-bay Model
Sampling speed	500Hz
Sampling time	30sec
Rise-span ratio h/L	0.1, 0.2, 0.3
Model scale	100mm x100mm (model : full =1:100)
Wall	Open type / Enclosed type
Wind direction	0-degree, 15-degree, 30-degree, 45-degree
Number of test on each model	Five times

Table 3. Model Condition

http://dx.doi.org/10.5772/54180

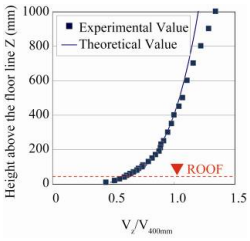

(a) Vertical Average Wind Speed Profile; Velocity gradient α=0.2 and wind velocity was about 7m/s at z=35mm

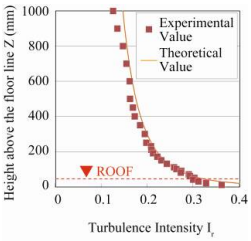

(b) Vertical Turbulence Intensity I_r Profile; I_r=0.3 at z=35mm

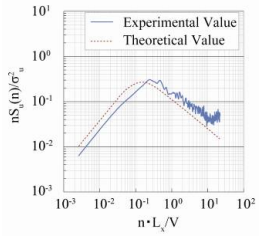

(c) Power Spectral Density of Fluctuating Wind Speed at z=30mm

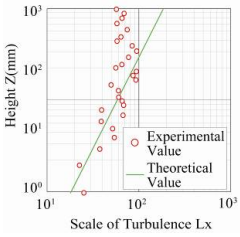

(d) Scale of Turbulence L_x

Figure 9. Wind flow conditions in the wind tunnel test

6. The wind tunnel test on the stand-alone model under the turbulent boundary layer flow

This chapter focuses on the stand-alone model of horn-shaped membrane roof and indicates wind pressure and fluctuating pressure around models under the boundary turbulent layer flow which was shown in the preceding section.

6.1. Outline of tests

The 100mm x 100mm square based model was used in this test. Major parameters were three types of rise-span ratio (h/L), namely h/L=0.1, 0.2 and 0.3, and the presence of walls. Six types of model were prepared for this wind tunnel test. The outline of models and measurement taps show in figure 10 and figure 11.

These models were made from acrylic plastic. As for the open type model, the roof depth was about 5mm in order to measure both sides of the roof at the same time (show in figure 12). Additionally, wind directions were only four types which were 0-deg., 15-deg., 30-deg. and 45-deg., because of symmetry form of roof.

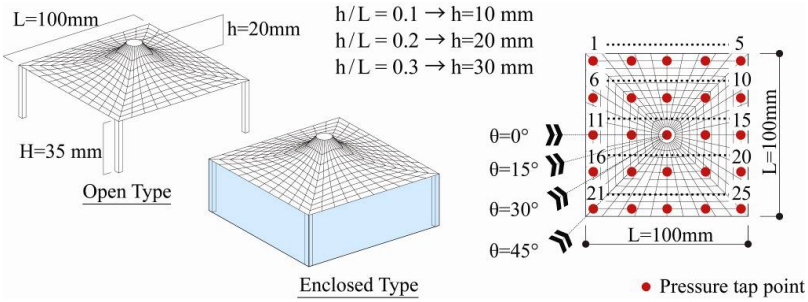

Figure 10. Experimental models and measuring points on the stand-alone models; two types model was prepared, namely "Open type" and "Enclosed type"

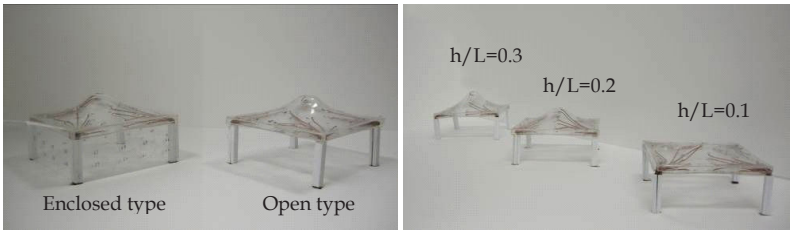

Figure 11. The photo of models; three types of h/L models which was made from acrylic plastic. The depth of open type's roof is about 5mm thick.

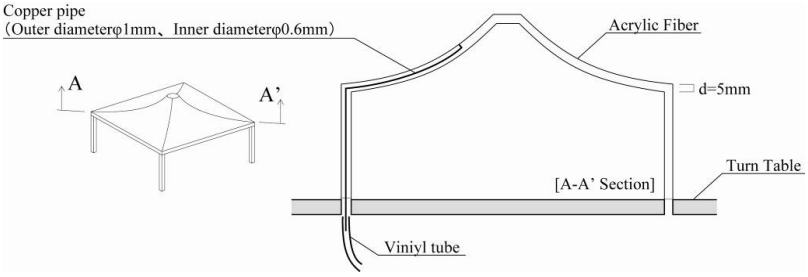

Figure 12. Details of the experimental model

6.2. Results of mean wind pressure coefficient on the stand-alone model

Distributions of mean wind pressure coefficient on each model are indicated in figure 13 and 14. The distribution of wind pressure coefficient changed the value depending on the presence of the wall. Similarly, the wind pressure coefficient distributions depended on the wind direction.

http://dx.doi.org/10.5772/54180

In the open type, the negative pressure concentrated at the windward side on the model. On the other hand, the negative pressure observed at the top of the roof on the enclosed model. Moreover, the negative pressure around the top of roof was increase with increasing of a rise-span ratio.

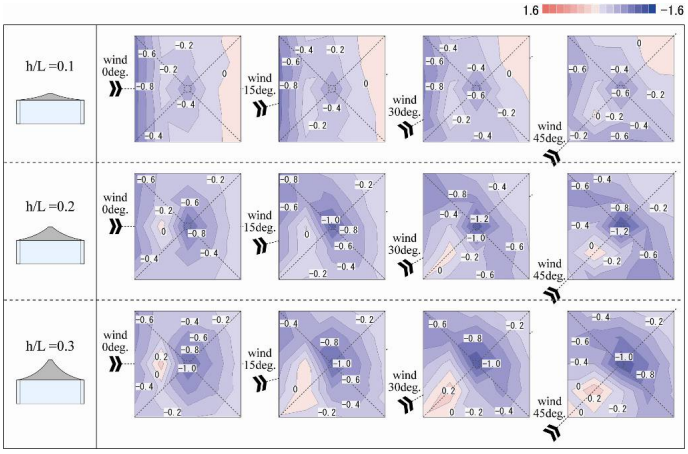

Figure 13. Mean wind pressure coefficient which was obtained from wind tunnel tests on enclosed type of the stand-alone mode

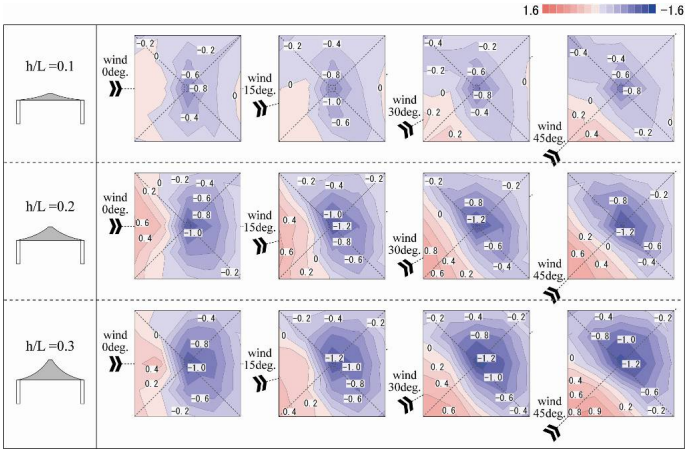

Figure 14. Mean wind pressure coefficient which was obtained from wind tunnel tests on open type of the stand-alone mode

6.3. Results of fluctuating wind pressure coefficient on the stand-alone model

This section shows the distributions of fluctuating wind pressure coefficient on each model (show in figure 15 and 16). The fluctuating wind pressure coefficient C_f' was obtained from the following equations;

$$C_f' = \frac{\sigma_p}{\bar{q}_z} \tag{9}$$

in which σ_p is fluctuating wind pressure at pressure tap p on the model and $\bar{q}_z$ is the mean value of dynamic velocity pressure at the reference location. The maximum value of the fluctuating wind pressure is "1.0" and the minimum value of the fluctuating wind pressure is "0".

The test result showed that the C_f' of the enclosed types were different distribution from the open types. Furthermore the C_f' of the enclosed type was larger than that of the open type. Especially, the model type h/L=0.2 of the enclosed model showed 0.75 around the center of the roof. These results may cause some effects on the response of membrane, since the membrane structure is generally sensitive structure for the external force such as wind load with turbulence.

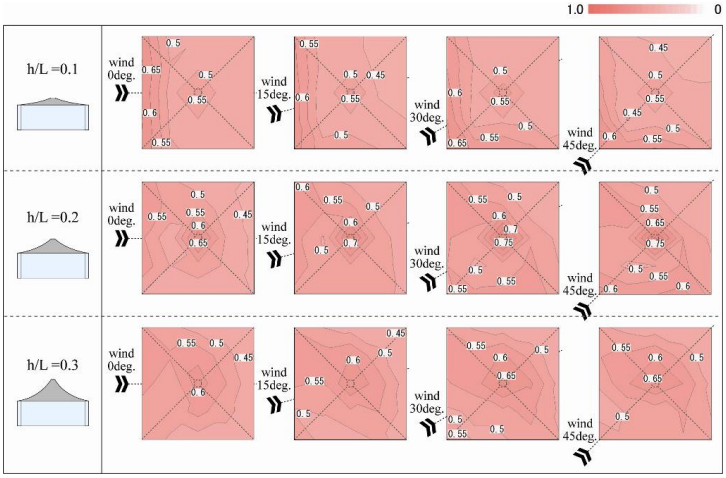

Figure 15. Fluctuating wind pressure coefficient which was obtained from wind tunnel tests on enclosed type of the stand-alone mode

6.4. Results of peak wind pressure coefficient on the stand-alone model

Distributions of the peak wind pressure coefficient on each model are indicated in figure 17 and 18. Generally, the peak wind pressures around corner of roof distinct from distributions

http://dx.doi.org/10.5772/54180

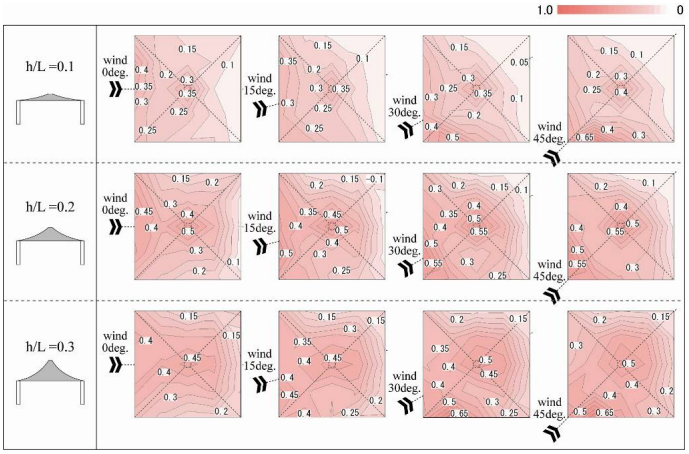

Figure 16. Fluctuating wind pressure coefficient which was obtained from wind tunnel tests on open type of the stand-alone mode

of the internal area. However, this test showed that peak wind pressure coefficients around the middle of roof (i.e. the top of roof) were the maximum negative value. In addition, the peak wind pressure coefficient of the enclosed model was larger than that of the open type. For example, focusing on the enclosed model, the model of h/L=0.2 and 0.3 show more than -4.0. Furthermore, the distribution varied according to the parameter of wind direction and rise-span ratio.

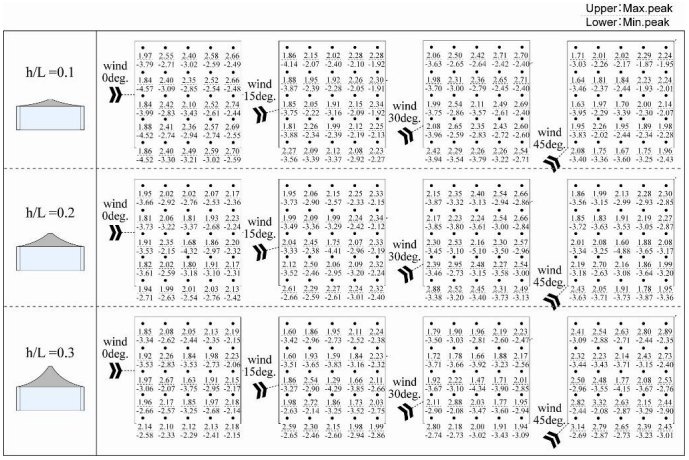

Figure 17. Peak wind pressure coefficient which was obtained from wind tunnel tests on enclosed type of the stand-alone mode

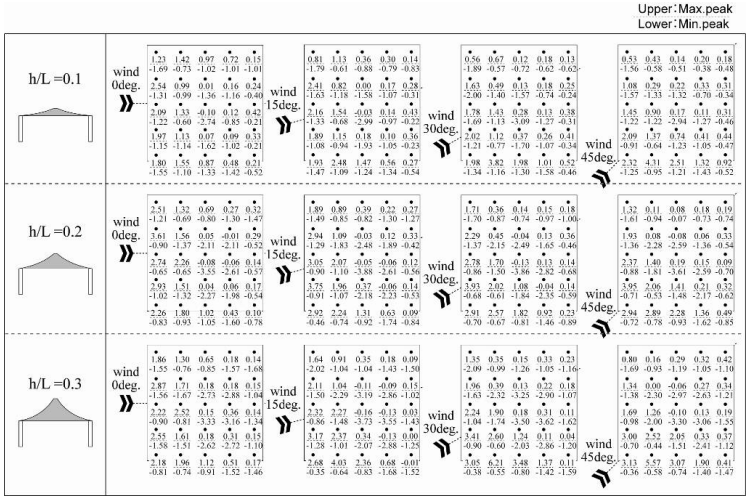

Figure 18. Peak wind pressure coefficient which was obtained from wind tunnel tests on open type of the stand-alone mode

7. The wind tunnel test on the multi-bay model under the turbulent boundary layer flow

In most cases, the horn shaped membrane structure is used as the multi-bay type. The number of horn unit depends on the scale of the building and the building uses. Therefore, this chapter focuses on the multi-bay model of 3×3. This test was carried out to clarify about the basic characteristics of the wind pressure coefficient of the multi-bay horn-shaped membrane roof.

7.1. Outline of tests

This test used the same facilities and the same turbulent flow as the stand-alone model shown in chapter 5. A model scale of a horn unit was 30cm x 30cm and the number of unit was 3 wide, 3 bays, and the models ware made from acrylic (see figure 19 and 20). This experimental model was only one type of rise-span ratio, namely h/L=0.2.

http://dx.doi.org/10.5772/54180

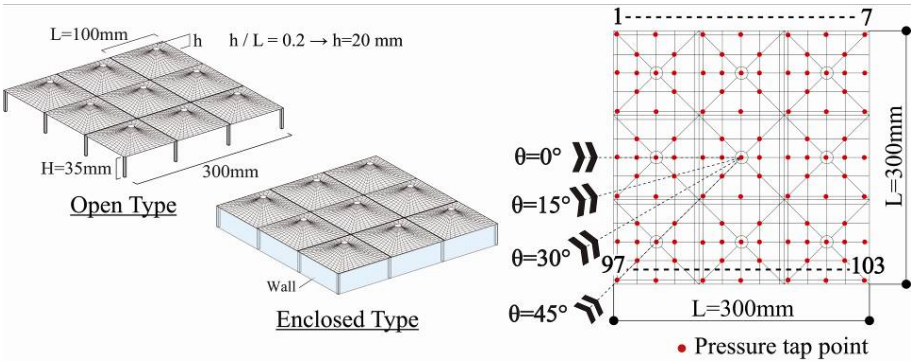

Figure 19. Experimental models and measuring points on the multi-bay models

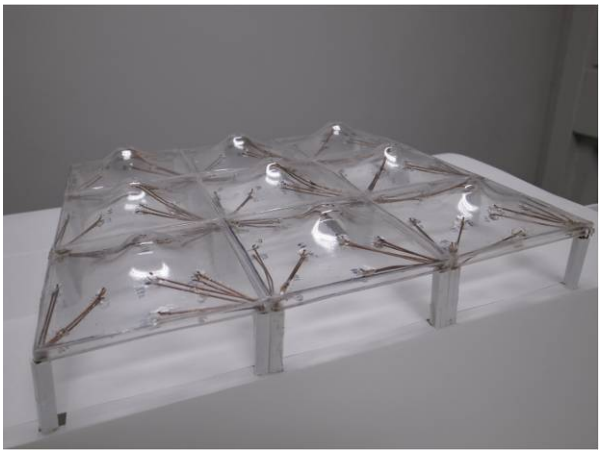

Figure 20. The photo of models on the multi-bay model; one type of h/L model which was made from acrylic plastic.

7.2. Results of mean wind pressure coefficient on the multi-bay model

Distributions of mean wind pressure coefficient on each model are shown in figure 21 and 22. The distributions were changed by wind direction as same as stand-alone models. Forcusing on the enclosed model, the positive pressure were shown around the valley of the roof. On the other hand, in the open type, windward side show positive pressure.

These results of open type were obtained approximately the same results with the stand-alone model of open type. On the other hand, as for the enclosed type, results were different from the stand-alone model. Specifically, focusing on the rise-span ratio 0.2, the value of the wind pressure coefficient around the middle of model was smaller than the stand alone models.

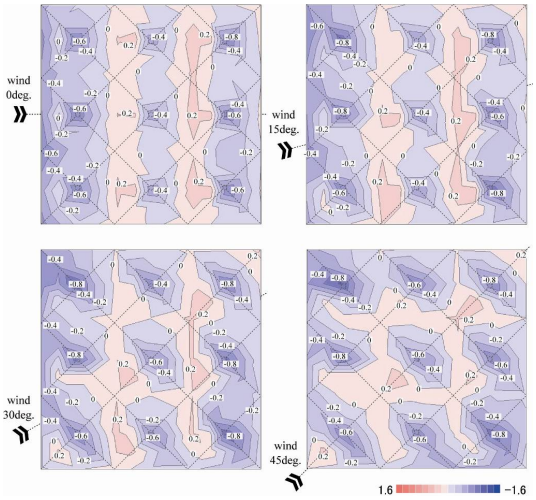

Figure 21. Mean wind pressure coefficient which were obtained from wind tunnel tests on enclosed type of the multi-bay mode

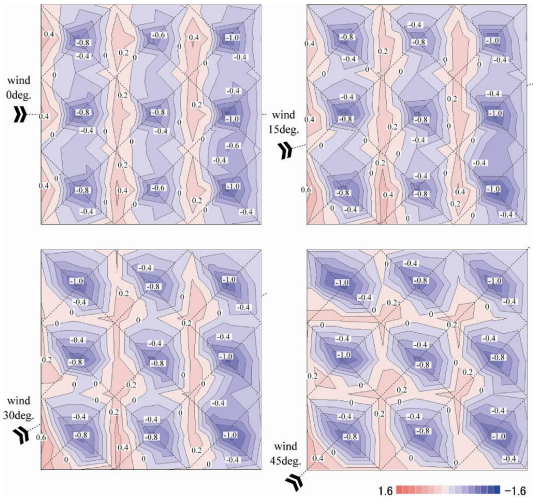

Figure 22. Mean wind pressure coefficient which were obtained from wind tunnel tests on open type of the multi-bay mode

7.3. Results of fluctuating wind pressure coefficient on the multi-bay model

Distributions of fluctuating wind pressure coefficient on each model are indicated in figure 23 and 24. The fluctuating wind pressure coefficients indicated on multi-bay model almost the

http://dx.doi.org/10.5772/54180

same as that on stand-alone model. The enclosed model showed value of 0.6 or more over the whole area of the roof. But the open type showed comparatively large value of approximately 0.8 on the only windward side.

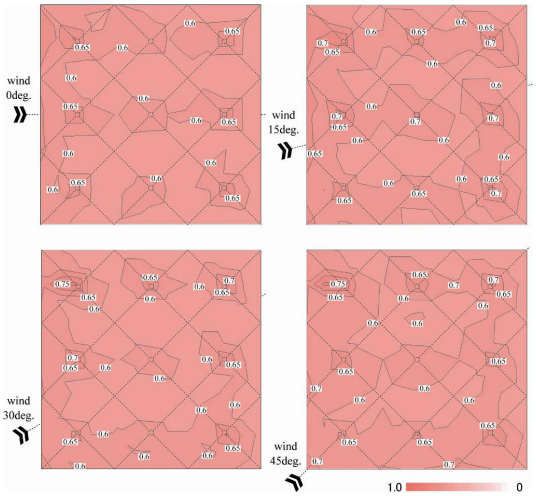

Figure 23. Fluctuating wind pressure coefficient which were obtained from wind tunnel tests on enclosed type of the multi-bay mode

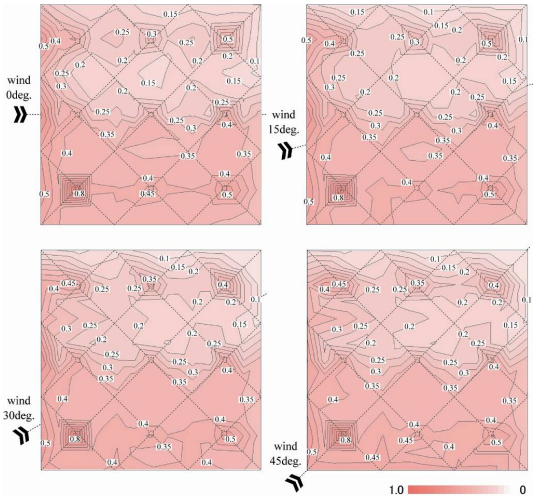

Figure 24. Fluctuating wind pressure coefficient which were obtained from wind tunnel tests on open type of the multi-bay mode

7.4. Results of peak wind pressure coefficient on the multi-bay model

The maximum peak wind pressure coefficients are shown in figure 25, and the minimum peak wind pressure coefficients are shown in figure 26. These distributions were changed by wind direction. Furthermore, these wind pressure coefficients around the top of roof indicated the maximum negative value. And these results were smaller than the stand-alone models.

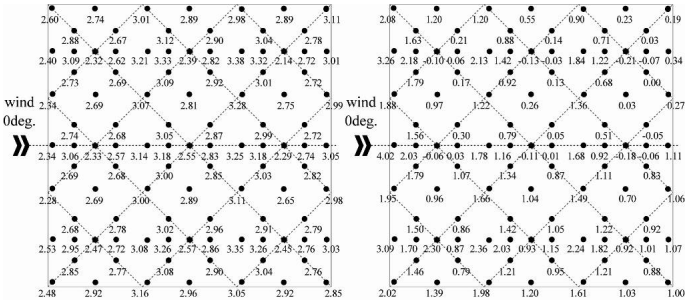

Figure 25. Maximum peak wind pressure coefficient which were obtained from wind tunnel tests on the multi-bay model

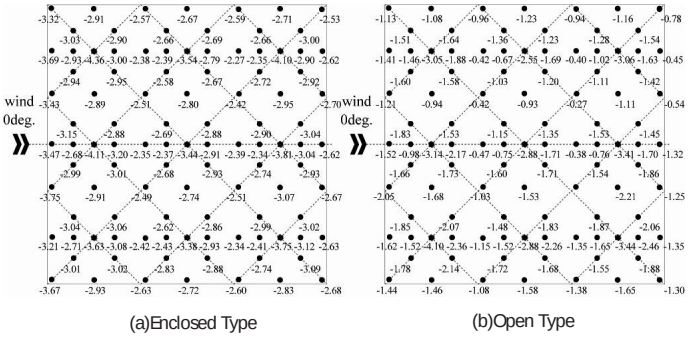

Figure 26. Minimum peak wind pressure coefficient which were obtained from wind tunnel tests on the multi-bay model

8. Conclusions

In this paper, the characteristics of the wind pressure coefficients on the horn-shaped membrane roof were presented using wind tunnel tests with the turbulent boundary layer flow. Particularly, the followings are clarified that;

http://dx.doi.org/10.5772/54180

- The wind pressure coefficient varied according to the presence of the wall and the wind direction.
- The negative pressure around the top of roof become larger with the increase of the rise-span ratio.
- The fluctuating wind pressure coefficient and the peak wind pressure coefficient on the enclosed type was larger than these of the open type.
- As for the mean wind pressure coefficient of the enclosed types, the multi-bay types were different from the stand-alone models. These results are forecast to cause unstable phenomenon of the membrane.

Furthermore, the representative distributions of the wind pressure coefficient were shown on each parameter.

Acknowledgements

This study was supported by Japan Society for the Promotion of Science, Grant-in-Aid for JSPS Fellows, KAKENHI 22・7895. All of tests were carried out on "Research Institute of Science and Technology, College of Science and Technology, Nihon University". The authors have had the support of Ayu Matsuda, Japan ERI Co.,Ltd., and Tomoaki Kaseya Graduate School of Science and Technology, Nihon University to carry out the experiments.

Author details

Yuki Nagai[1], Akira Okada[2], Naoya Miyasato[2], Masao Saitoh[2] and Ryota Matsumoto[2]

1 Sasaki Structural Consultants, Japan

2 Nihon University, Japan

References

[1] Architectural Institute of Japan, *Recommendations for Load on Buildings. (2004)*, Architectural Institute of Japan, ISBN 481890556,Japan

[2] The building Center of Japan. (2004). *The Building Standard Law of Japan June 2004*, The building Center of Japan. , ISBN 4-88910-128-4, Japan

[3] Cermak, J.E. & Isyumov, N., with American Society of Civil Engineers Task Committee. (1998), *Wind Tunnel Studies of Buildings and Structures (Asce Manual and Reports on Engineering Practice)*, American Society of Civil Engineers, ISBN 0784403198

[4] Cook, N.J. (1990), *Designer's Guide to Wind Loading of Building Structures Part 2: Static structures*, Laxton's, ISBN 0408008717

[5] Forster, B. et al. (2004), *European Design Guide Tensile Surface Structures*, TensiNet, ISBN 908086871

[6] Kaiser, U. (2004), *Wind Wirkung auf Schwach Vorgespannte membran strukturen am beispiel eines 30m-membranschirmes*, Der Andere Verlag., ISBN 3899591623, Germany

[7] Ma, J., Zhou, D., LI, H., ZHU, Z. & DONG, S. *Numerical simulation and visualization of wind field and wind load on space structure*, Proceedings of IASS 2007, Beijing, 2007

[8] Nerdinger, W. (2005). *Frei Otto Complete Works: Lightweight Construction Natural Design*, Birkhäuser Architecture, ISBN 3764372311

[9] Janberg, N. (2011). BC Place stadium, In: *Nicolas Janberg's Structurae,* March 21, 2011, Available from: http://en.structurae.de/structures/data/index.cfm?id=s0000708

[10] Janberg, N. (2011). Lord's Cricket Ground Mound Stand, In: *Nicolas Janberg's Structurae,* March 21, 2011, Available from: http://en.structurae.de/structures/data/index.cfm?id=s0000694

[11] Otto, F. (1969). *Tensile Structures: Cables, Nets and Membranes v. 2*, MIT Presse, ISBN 0262150085, USA

[12] Saitoh, M. (2003). *Story of Space and Structure -Structural Design's Future*, Shoukokusha, ISBN 4395006396, Japan

[13] Saitoh, M. & Kuroki, F. *Horn Type Tension Membrane Structures,* Proceedings of IASS 1989, Madrid, 1989

[14] Seidel, M. & David, S. (2009). *Tensile Surface Structures - A Practical Guide to Cable and Membrane Construction: Materials, Design, Assembly and Erection*, Wiley VCH, ISBN 3433029229, Germany

[15] Shinkenchiku-Sha Co. Ltd. (1992). Hyper Dome E, In: *Shinkenchiku March,1992*, Shinkenchiku-Sha Co. Ltd. ISSN 1342-5447, Japan

[16] Shinkenchiku-Sha Co. Ltd. (1988). Tokyo Dome, In: *Shinkenchiku May, 1988*, Shinkenchiku-Sha Co. Ltd. ISSN 1342-5447, Japan

[17] Shinkenchiku-Sha Co. Ltd. (2007). BDS Kashiwanomori Auctionhouse, In: *Shinkenchiku October, 2007*, Shinkenchiku-Sha Co. Ltd. ISSN 1342-5447, Japan

[18] Wang, C., Zhou, D. & Ma, J. *The interacting simulation of wind and membrane structures*, Proceedings of IASS 2007, Beijing, 2007

http://dx.doi.org/10.5772/54180

[19] Nagai, Y. Et al. *Wind Response on Horn-Shaped Membrane Roof and Proposal of Gust Effect Factor for Membrane Structure,* Proceedings of IASS 2012, Seoul, 2012